

RESEARCH PAPER

## Synthesis and evaluation of SPION@CMD@Ser-LTVSPWY peptide as a targeted probe for detection of HER2+ cancer cells in MRI

Arash Papi<sup>1</sup>, Rasoul Irajirad<sup>2</sup>, Milad Yousefvand<sup>1</sup>, Alireza Montazerabadi<sup>1\*</sup>, Zahra Mohammadi<sup>3\*\*</sup>

<sup>1</sup>Medical Physics Research Center, Mashhad University of Medical Sciences, Mashhad, Iran

<sup>2</sup>Finetech in Medicine Research Center, Iran University of Medical Sciences, Tehran, Iran

<sup>3</sup>Radiological technology department of actually paramedical sciences, Babol University of medical sciences

### ABSTRACT

**Objective(s):** Successful detection of tumors in the early stages can significantly increase a patient's healing process and recovery speed. Conventional imaging techniques usually depend on the tissues' anatomical structure. Epidermal growth factor receptor-2 (HER-2) is a transmembrane protein with an extracellular ligand-binding domain. HER2 plays an essential role in cell proliferation, differentiation, and survival, and its overexpression is associated with various cancers, especially breast and ovarian cancers. Access to its extracellular domain makes HER2 an ideal target for drug preparation and molecular imaging probes. In this study, a targeted magnetic nanoprobe for molecular imaging of HER2 positive cancers was synthesized, and also its potential as a T<sub>2</sub>-weighted targeted contrast agent was assessed.

**Materials and Methods:** Superparamagnetic SPION nanoparticles were synthesized using the co-precipitation method in the presence of CMD and were labeled with SLTVSPWY peptide. The SPION@CMD@SLTVSPWY nanocomplex was characterized by TEM, DLS, XRD, AAS, FTIR, EDX, and VSM. The r<sub>1</sub> and r<sub>2</sub> relaxivities were then calculated using a 1.5 Tesla clinical magnetic field. The cytotoxicity of the nanocomplex was evaluated by MTT assay. Finally, the difference between uptake of targeted nanocomplexes and SPION by the human SKOV-3 cell line (HER2 +) was investigated.

**Results:** The SPION@CMD NPs were synthesized with spherical shape and superparamagnetic behavior. Characterization results confirmed the formation of SPION@CMD@SLTVSPWY. r<sub>2</sub> relaxivity and r<sub>2</sub>/r<sub>1</sub> calculations resulted in suitable values of 313 mM<sup>-1</sup>s<sup>-1</sup> and 8.05 for SPION@CMD@SLTVSPWY, respectively. Increased uptake of targeted nanocomplexed (SPION@CMD@SLTVSPWY) compared to non-targeted NPs (SPION@CMD) was very noticeable visually, and its numerical ratio was 3.51 at a concentration of 0.075 mM.

**Conclusion:** The targeted synthesized nanocomplex in this study has great potential as a T<sub>2</sub> weighted probe contrast agent in MR imaging owing to its appropriate high uptake in HER2 + cells.

**Keywords:** Cancer; HER2 receptor; LTVSPWY peptide; MRI; SKOV-3; SPION

### How to cite this article

Papi A, Irajirad R, Yousefvand M, Montazerabadi AR, Mohammadi Z. Synthesis and evaluation of SPION@CMD@Ser-LTVSPWY peptide as a targeted probe for detection of HER2+ cancer cells in MRI. *Nanomed J.* 2021; 8(4): 279-289. DOI: [10.22038/NMJ.2021.59629.1614](https://doi.org/10.22038/NMJ.2021.59629.1614)

### INTRODUCTION

Successful early tumor detection at the earliest possible stage or even at the precancerous lesion stage or the "Stage 0" can significantly improve the patient's healing process and recovery (1, 2). Conventional clinical imaging techniques are commonly used to detect lesions

larger than 1 cm in diameter (3, 4). Therefore, there has been an urgent need to develop precise methods for early detection and enhance anti-tumor drugs specificity (4, 5). In this regard, cellular and molecular imaging plays an essential role in preventing disease and improving treatment efficiency by detecting the cell's fate, signaling paths, growth factors, and other mechanisms. Molecular cell imaging indirectly measures the biological and cellular processes of the body for diagnostic and therapeutic applications. Therefore, it has a unique ability to describe body tissues

\* Corresponding Author Email: [alireza.montazerabadi@gmail.com](mailto:alireza.montazerabadi@gmail.com), [mehr\\_055@yahoo.com](mailto:mehr_055@yahoo.com)

Note. This manuscript was submitted on October 10, 2020; approved on January 10, 2021

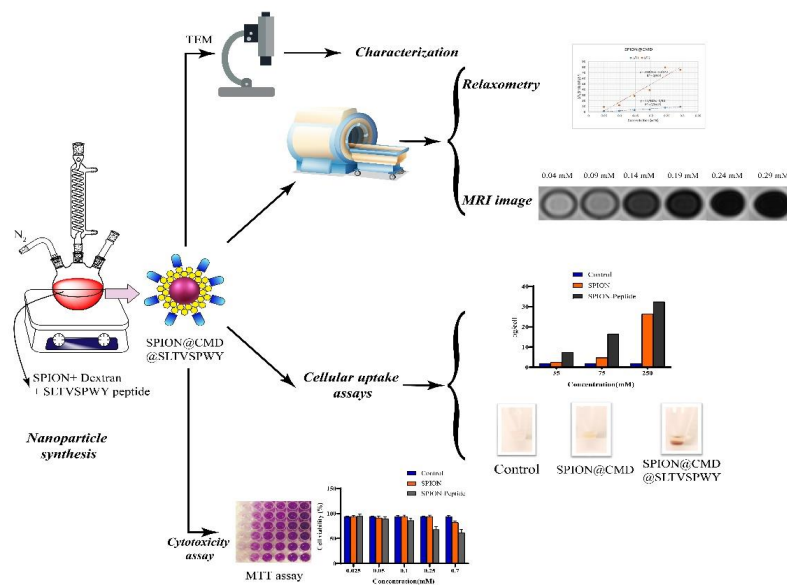


Fig 1. Schematic illustration of SPION@CMD@ SLTVSPWY as a targeting system for MRI

pathology without invasive procedures(6, 7). The purposes of molecular researches are detecting factors that help tumor growth, proliferation, angiogenesis, metastases, developing diagnosis and treatment tools by targeting methods. Molecular imaging probes can help visualize and quantify cancer's anatomical, functional and molecular profiles (4).

Some cancers are associated with increased expression of cell surface receptors. Among them is the human epidermal growth factor receptor 2 (HER2)(8). human epidermal growth factor receptor 2 (HER-2 or ErbB2) is a transmembrane protein capable of attaching to extracellular N-terminal ligand and intracellular tyrosine kinase. HER2 receptor expression can cause epithelial-like cancers, such as uterine, ovarian, breast, lung, prostate, intestine, stomach, kidney, and pancreas cancers (8). HER2 plays an essential role in cell proliferation, differentiation, and survival. Its expression is intensively related to tumor aggressiveness, recurrence risk, and weak prognosis. As a result, HER2 is an effective indicator of cancer diagnosis and treatment(9). Due to its extracellular domain, HER2 is becoming an ideal target for drug preparation and cellular and molecular imaging (10).

Today, Receptor-mediated tumor targeting has been considered because of its high specificity (11). A critical aspect for the successful progress of targeted drug delivery is based on discovering particular ligands. Peptides targeting are ligands with low molecular weight and high cell/tissue penetration. These features make the peptides recognized as promising candidates for diagnosis

and treatment of cancer (2, 12, 13). Heptapeptide LTVSPWY has a high binding specificity for HER2 receptors (14-20). Recently, Superparamagnetic iron oxide particles (SPION) are being used as a theranostic agent in various imaging modalities, including magnetic resonance imaging (MRI), magnetic particle imaging (MPI) and treatment modality of magnetic induction hyperthermia(11, 21, 22). Despite the mentioned advantages of iron oxide application, the necessity of injection high doses of the MNPs (SPION) for effective MRI and magnetic hyperthermia is the most crucial disadvantage. Simultaneously, this procedure causes high accumulation in non-target tissues, toxicity, temperature rise, and noise in background tissue. High dose injection of the MNPs leads to undesirable results and sometimes patient intolerance (11). A targeted drug delivery method can be used to prevent such consequences. This study constructs a specific contrast agent for HER2-positive cancers. In this regard, magnetic iron oxide nanoparticles were coated by carboxymethyl dextran (CMD) and marked by anti-HER2 peptides (LTVSPWY). Then, the performance of the nanocomplex as a targeted contrast probe was investigated.

## MATERIAL AND METHODS

Ser-LTVSPWY-COOH peptide was synthesized by HuiChem (China) and purchased. Dextran,  $\text{FeCl}_2 \cdot 4\text{H}_2\text{O}$ , 99%, Sodium hydroxide (NaOH), bromoacetic acid,  $\text{NH}_4\text{OH}$  (5 M), 2,5-diphenyltetrazolium bromide (MTT) were purchased (Sigma Aldrich). Neodymium magnet

N50 (50× 50 × 30 mm) with 14 kg of Gauss remanence was purchased (Iran). Fetal bovine sera (FBS), trypsin, Cell culture media (RPMI1640), and streptomycin solution were purchased from Gibco (Germany). SKOV-3 human ovarian carcinoma cell line was obtained from the Pasteur Institute of Iran and the National Center of Genetic of Iran.

#### **Synthesis of nanocomplex SPION@CMD@Ser-LTVSPWY-COOH**

##### **Preparation of carboxymethyl dextran (CMD)**

To prepare CMD, 1 gr of dextran was dissolved in 3 ml of distilled water, then 3 ml of NaOH (8 M) was added, and the reaction solution temperature was raised to 60-65 ° C by a hot water bath. 0.4 gr of Bromoacetic acid was added. Then, the mixing reaction continued at this temperature for 2 hr. After this time, the reaction solution was neutralized by adding acid, and the dextran was washed with ethanol three times. Finally, it dried at 60 ° C.

##### **Synthesis of iron oxide magnetic nanoparticles in the presence of CMD**

In order to synthesize SPION@CMD, 1 gr of CMD produced according to the previous protocol was dissolved in 25 ml of water and then was filtered by a 0.2-micron syringe filter. 0.75 gr of FeCl<sub>3</sub>.6H<sub>2</sub>O salt and 0.4 gr of FeCl<sub>2</sub>.4H<sub>2</sub>O salt were dissolved in 10 ml of water and filtered by a 0.2-micron syringe filter. CMD solutions and iron salts were mixed together, and the solution temperature reached 10 ° C. 2.83 ml of 28% ammonia (NH<sub>3</sub>) was added dropwise until the black iron oxide formation. This product was kept at 78 ° C for one hour. After cooling at room temperature, it was neutralized by acetic acid. Large particles were separated by 1500 rpm for 15 min. The supernatant was dialyzed for one day by a 20 kDa dialysis bag after centrifugation.

##### **Labelling SPION@CMD with peptide Ser-LTVSPWY-COOH**

2 ml of the SPION@CMD synthesized with concentration of 5000 ppm was placed on the stirrer and 0.0211 gr of Na<sub>2</sub>CO<sub>3</sub> was added while the pH reached about 10. After dissolution, 4.6 mgr Cyanogen bromide (CBrN) was added. After 10 min, 0.0238 gr of sodium dihydrogen phosphate (Na<sub>2</sub>HPO<sub>4</sub>) was added until the pH reached about 8.5. Then, 4.8 mgr of the peptide was added and rotated at room temperature for 2 hr. Then, 3.2 mgr of glycine was added to the reaction solution, and the temperature was set to 6 ° C for 24 hr. In the last step, it was dialyzed for one day by a 20 kDa dialysis bag.

#### **Physico-chemical characterizations**

##### **Dynamic Light Scattering (DLS)**

The hydrodynamic particle size, size

distributions, and zeta potential of SPION@CMD@SLTVSPWY and SPION@CMD were measured by the DLS system using a HORIBA Zetasizer (NANO-ZS, Malvern, UK).

##### **Transmission Electron Microscopy (TEM)**

The morphology and size distribution of the synthesized nanoparticle was evaluated with the TEM system. A 100 KeV field emission Philips CM120, Philips Electron Optics, Netherland was used to get TEM.

##### **Phase structure**

To confirm the crystal structure of SPION, the X-ray diffraction (XRD) (GNR EXPLORER, Italy) was performed approximately equal to room temperature (25° C). For this purpose, the XRD system was set to the 20<sup>o</sup>–80<sup>o</sup> (2θ) range that using Cu-Kα (with λ= 1.54 Å, 40 kV, 30 mA) of radiation parameter.

##### **Infrared spectra**

Fourier-transform IR (FTIR) spectroscopy was used to identify functional groups and chemical structural changes in SOION@CMD@SLTVSPWY and SPION@CMD.

##### **Magnetometry**

vibrating sample magnetometer (vibrating sample magnetometer) VSM (VSMF model, Iran) was used to obtain the magnetic field-dependent magnetisation loop from -10000 to 10000 Oe at room temperature.

##### **Relaxivity measurements**

Magnetic nanoparticles as a contrast agent in MRI could change relaxation times (T<sub>1</sub> and T<sub>2</sub>). Iron oxide-based MNPs are often used to enhance T<sub>2</sub> contrast is referred to as T<sub>2</sub> weighted images. r<sub>1</sub> and r<sub>2</sub> quantify the contrast-enhancing efficiency of contrast agents. (longitudinal and transversal relaxivities values). r<sub>1</sub> and r<sub>2</sub> were calculated by relaxometry of phantom containing the synthesized nanostructures at 1.5 Tesla MRI scanner (Avanto/ SIEMENS) at various Fe concentrations of (0.045, 0.091, 0.137, 0.183, 0.229, and 0.275 mM) according to AAS results. T<sub>1</sub>-weighted images were obtained at Time of Repetition (TR): 100 to 2000 ms: 100/300/600/900/1200/2000 ms; Time of Echo (TE): 8.7 ms; flip angle: 20 degrees; the field of view(FoV): 260 mm; matrix size: 256× 192; 100%; averages: 1, echo train length: 1; slice thickness: 5 mm. T<sub>2</sub>-weighted images were acquired with T<sub>2</sub> spin-echo multi-section pulse sequence by TE, 13.8 to 165.5: 13.8/27.9/41.4/55.2/69.0/82.8/96.6/110.4/124.2/138.0/151.8/165.6/ 179.4/193.2/207.0/220.8 ms; TR of 2000 ms; ; matrix size: 256 ×192; flip angle:

20 degree FoV: 260 mm; 100%; averages: 1, echo train length: 1. The data analysis and curves fitting was performed by using Origin pro radiant Dicom viewer software and Excel.

### Cytotoxicity assay

Cytotoxicity of the nanostructures was assessed using the MTT assay. Briefly, the SKOV-3 cells were seeded in 96-well plates at a density of  $8 \times 10^3$  cells/well and incubated at 37°C and 5% CO<sub>2</sub> for 24 hr. In the next step, the cells were exposed to various concentrations (0.025, 0.05, 0.1, 0.25, and 0.7 mM) of SPION@CMD and SPION@CMD@SLTVSPWY for 24 hr in the incubator. Finally, the MTT assay was carried out to estimate the cell viability.

### Quantitative evaluation of cell uptake in vitro

The amount of absorbed iron was measured quantitatively in cells incubated with nanocomplexes SPION@CMD and SPION@CMD@SLTVSPWY. Briefly, SKOV-3 cancer cells were cultured in 6-well plates with a seeding density of  $4 \times 10^5$  cells/well for 24 hr. After washing, the cells were incubated with synthesized nanostructures (SPION@CMD@SLTVSPWY and SPION@CMD) at concentration of 0.035, 0.075, and 0.25 mM for 24 hr (concentration series of nanostructures were measured and used based on the iron content in it with the help of atomic absorption spectroscopy (AAS)). In the next step after washing the cells three times with PBS, complete cellular digestion was carried out by using perchloric acid. Finally, the iron (Fe) concentration of the cells was measured by AAS.

### Visual evaluation of cell uptake in vitro

The visual technique was used to visualize the

accumulation of synthesized nanostructures in SKOV-3 cells. SKOV-3 cells ( $4 \times 10^6$ ) were cultured in three single T75 flasks for 24 hr at 37°C incubators. Then, the cells were incubated with SPION@CMD and SPION@CMD@SLTVSPWY at a concentration of 0.25 mM for 24 hr. After washing with PBS and separation from the flasks, the cells were centrifuged in falcon.

## RESULTS

### Synthesis and Physico-chemical characterizations of Nanoparticles

Fig 2. shows a schematic scheme of the nanocomplex synthesis steps and interactions of the components. The reaction of dextran with bromoacetic acid produced dextrin carboxylate. To synthesize SPION nanoparticles, Iron (III) chloride and iron (II) chloride simultaneously reacted with dextrin carboxylate prepared in the previous step. Simultaneous synthesis of iron oxide nanoparticles in the presence of dextrin carboxylate has two advantages: The first is that dextran forms a stable bond with nanoparticles due to carboxyl groups. The second is that it causes a more uniform size distribution in the formation of nanoparticles. After the formation of dextran-coated nanoparticles, they react with Cyanogen bromide (CBrN). Cyanogen bromide reacts with groups OH of dextran on the one hand and can form an amide bond with the peptide amine group on the other hand. An LTVSPWY peptide was used in this study, and a Serine amino acid was added to its N- terminus as a spacer. The N- terminus of peptide reacted with Cyanogen bromide in the last step, and the final complex was formed.

FTIR. Fig 3. shows the FTIR results of

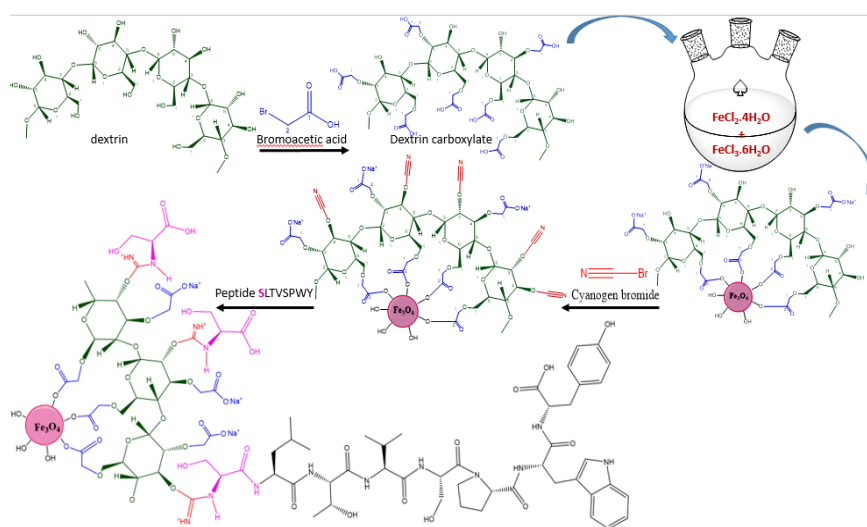


Fig 2. Synthetic scheme of SPION@CMD@SLTVSPWY

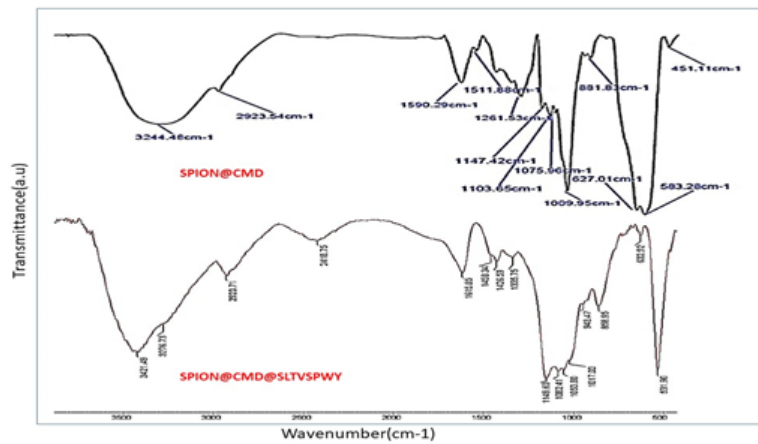


Fig 3. FTIR spectra of SPION@CMD@SLTVSPWY and SPION@CMD

nanostructures SPION@CMD@SLTVSPWY and SPION@CMD. In the spectrum related to SPION@CMD nanostructure, the band at 3244  $\text{cm}^{-1}$  is associated with the stretching vibration and bending vibration of the O-H bonds is associated with the adsorbed water groups. The peaks at 2923  $\text{cm}^{-1}$  and 583  $\text{cm}^{-1}$  were associated with the  $\text{CH}_2$  and C-O bonds of CMD, respectively. The peak at 583  $\text{cm}^{-1}$  is related to Fe-O bonds. Also, the peak at 1590  $\text{cm}^{-1}$  is associated with the carbonyl of the asymmetric carboxyl group. In the spectrum of SPIONs coated with peptide SLTVSPWY, Peak at 3421  $\text{cm}^{-1}$  is associated with the O-H bond of CMD and water while amine bonds overlap. The peak at 2418  $\text{cm}^{-1}$  is associated with nitrile bond, 1615

$\text{cm}^{-1}$  peak is associated with the formed amide group's carbonyl, 1149  $\text{cm}^{-1}$  is associated to the C-N peptide bond, 1082  $\text{cm}^{-1}$  peak is associated to C-O bond of CMD and peak at 531  $\text{cm}^{-1}$  is associated with Fe-O bond of iron oxide nanoparticles.

**DLS.** The results of SPION@CMD@SLTVSPWY and SPION@CMD nanocomplexes were shown as single castles (Fig 4). The highest frequencies of SPION@CMD@SLTVSPWY and SPION@CMD were 162.9 and 160.8 nm, respectively (Fig 4a, 4b). Zeta potential was measured at -75.9 mV for SPION@CMD and -6.5 mV for SPION@CMD@SLTVSPWY (Fig 4c).

**TEM.** The TEM image taken from SPION@CMD shows a spherical structure (Fig 5a). The histogram

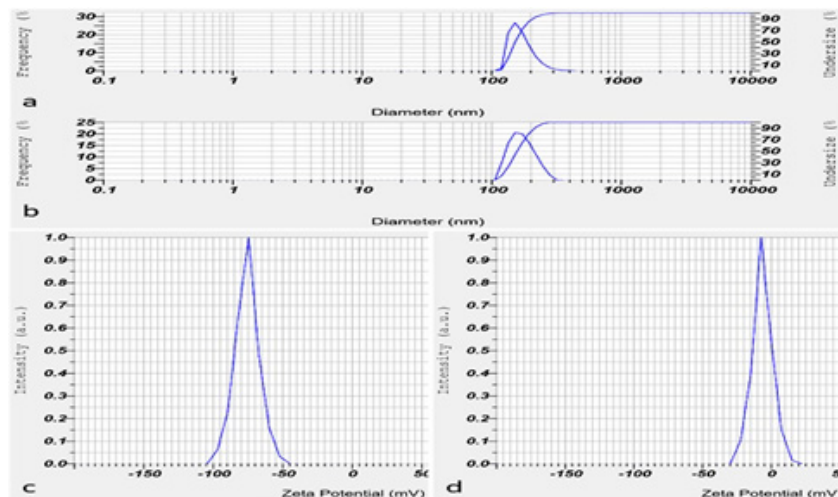


Fig 4. The hydrodynamic particle size distribution diagram. SPION@CMD(a) and SPION@CMD@SLTVSPWY(b); peaks at 160.8 nm and 162.9 nm, respectively zeta potential map of SPION@CMD(c), and zeta potential map of SPION@CMD@SLTVSPWY(d) were measured at -75.9 mV and -6.5 mV, respectively

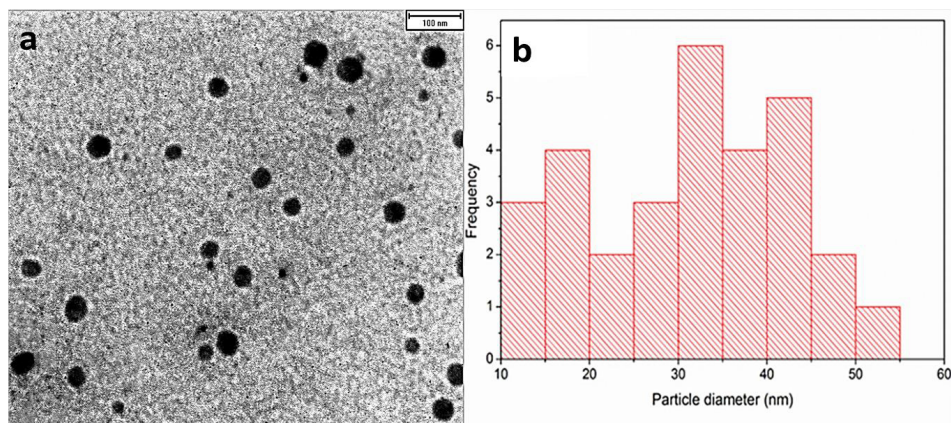


Fig 5. (a) TEM images of SPION@CMD (b) Size distribution histogram of SPION@CMD

of nanoparticle size distribution showed that the maximum SPION@CMD is approximately between 30 and 45, with an average size of 31.35 nm in diameter (Fig 5b).

**XRD.** XRD pattern of the SPIONs is shown in Fig 6. Based on this pattern, the maximum diffraction peak occurred at a  $2\theta$  value of  $35.7^\circ$ . All peaks' location and relative intensity were matched well with the pattern of standard magnetite SPION (JCPDS card, file No. 19-0629), denoting that the synthesized SPION are magnetic crystals. The Scherrer's equation estimated the mean crystal size (D):  $D = K\lambda/\beta \cos\theta$  where K is the Scherrer constant,  $\lambda$  is the wavelength,  $\beta$  is the FWHM (in radians), and  $\theta$  is the peak angular position. As a result, the crystal size of the SPION was calculated by the highest intensive peak (311) with a value of  $\sim 7.95$  nm. The peaks of the crystalline pattern of hydrophobic SPIONs are related to the 220, 311, 400, 422, 511, and 440 planes of x-ray diffraction (23).

**VSM.** The magnetic properties of SPION@CMD were investigated using a SQUID system. (Fig 7).

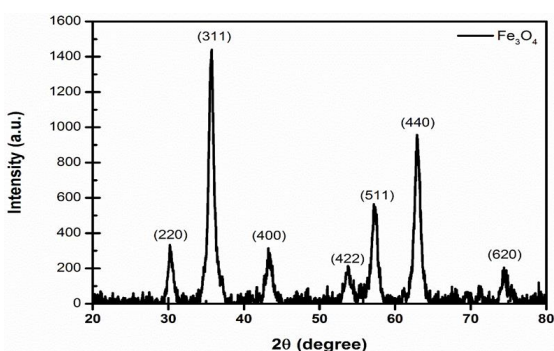


Fig 6. XRD pattern of SPION sample synthesized by a co-precipitation method. The XRD system acted at 40 kV and 30 mA in a  $2\theta$  range of  $20^\circ$ - $80^\circ$

According to this hysteresis curve,  $M_r$  and  $H_c$ 's zero values in the curve confirm the superparamagnetic behavior of the synthesized SPION@CMD. The results showed that SPION@CMD has a saturation magnetization of 18.26 emu/g at  $27^\circ\text{C}$ .

#### MRI Relaxometry

The properties of magnetic relaxation were analyzed to evaluate the potential application of nanocomplexes as MR contrast agents.  $T_1$  and  $T_2$  - weighted images were taken using aqueous suspensions of the nanocomplexes at concentrations 0.045, 0.091, 0.137, 0.183, 0.229 and 0.275 mM of Fe. For nanostructure SPION@CMD, the values of  $r_2$  and  $r_1$  were calculated as 318.16 and  $34.40 \text{ mM}^{-1}\text{s}^{-1}$ , respectively (Fig 8). In comparison, the values  $r_2$  and  $r_1$  for SPION@CMD@SLTVSPWY were calculated as 313.26 and  $38.91 \text{ mM}^{-1}\text{s}^{-1}$ , respectively (Fig 9). The  $r_2/r_1$  ratio is an interesting, sensitive parameter used to identify the contrast agents' category ( $T_1$  or  $T_2$  contrast agent). The  $r_2/r_1$  ratio was calculated

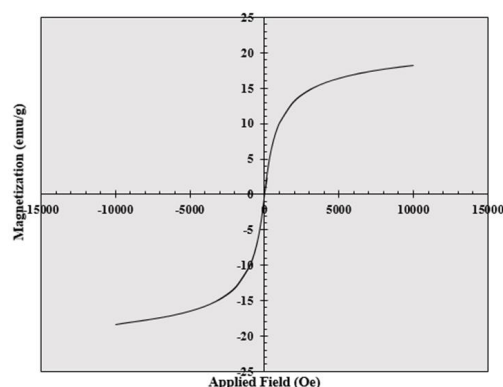


Fig 7. The magnetic hysteresis curve for SPION@CMD at the magnetic field ranges from 0 to 10 kOe at  $27^\circ\text{C}$

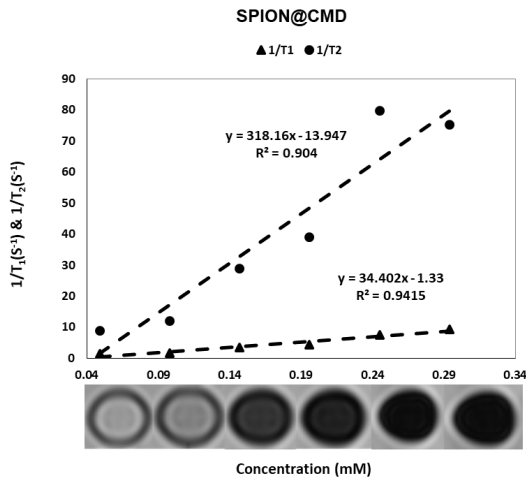


Fig 8. Longitudinal ( $r_1$ ) and transverse( $r_2$ ) relaxivity plot of the aqueous suspension of SPION@CMD

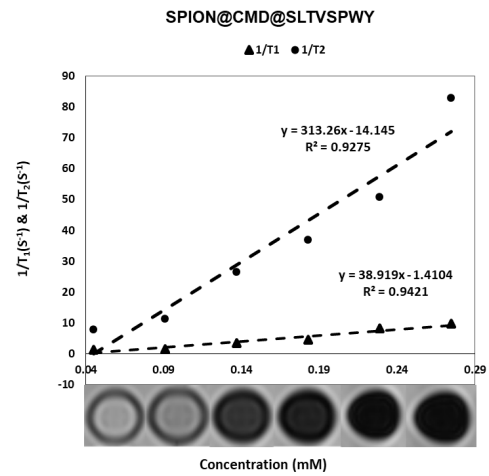


Fig 9. Longitudinal and transverse relaxivity plot of the aqueous suspension of SPION@CMD@SLTVSPWY

as 9.24 and 8.05 for SPION@CMD and SPION@CMD@SLTVSPWY, respectively.

#### Cell viability assay of nanoparticles

The cytotoxicity of SPION@CMD@SLTVSPWY and SPION@CMD was investigated by MTT assay (Fig 10). The cytotoxicity of the nanocomplexes was investigated on the SKOV-3 cell line at concentrations of 0.025, 0.05, 0.1, 0.25, and 0.7 mM for 24 hr. Using SPSS software, the data normality was checked based on the Kolmogorov–Smirnov test ( $*P > 0.05$ ). Then the homogeneity of variance of the groups was examined. The ANOVA test results showed a significant difference between the groups and the control group ( $*P < 0.05$ ). Due to the equality of variances ( $P$ -value=0.093),

the Dunnett test was used to compare groups. Mean cell survival percentage at 0.025, 0.05, 0.1, 0.25 mM concentrations of SPION@CMD and 0.025, 0.05, 0.1 mM concentrations of SPION@CMD@SLTVSPWY does not show any significant difference compared to the control group. However, SPION@CMD concentration of 0.7 mM and SPION@CMD@SLTVSPWY concentrations of 0.25 and 0.7 mM showed a significant difference compared to the control group. This toxicity and reduced survival may be due to the high uptake of the nanocomplex by the receptor into the cell.

#### Quantitative evaluation of cell uptake in vitro

The atomic absorption spectroscopy (AAS) test results of measuring the amount of iron-loaded inside SKOV-3 cells showed a significant increase

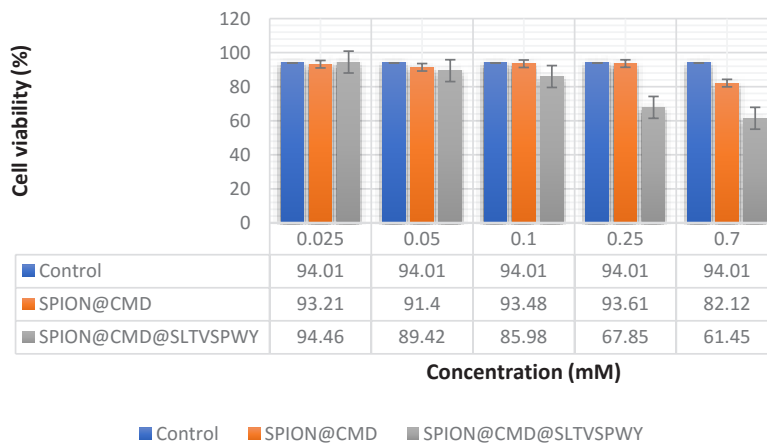


Fig 10. *In vitro* cytotoxicity of SPION@CMD@SLTVSPWY and SPION@CMD tested on SKOV-3 cell line after 24 h incubation at 37 °C. Data are shown as mean  $\pm$  SD (n = 5)

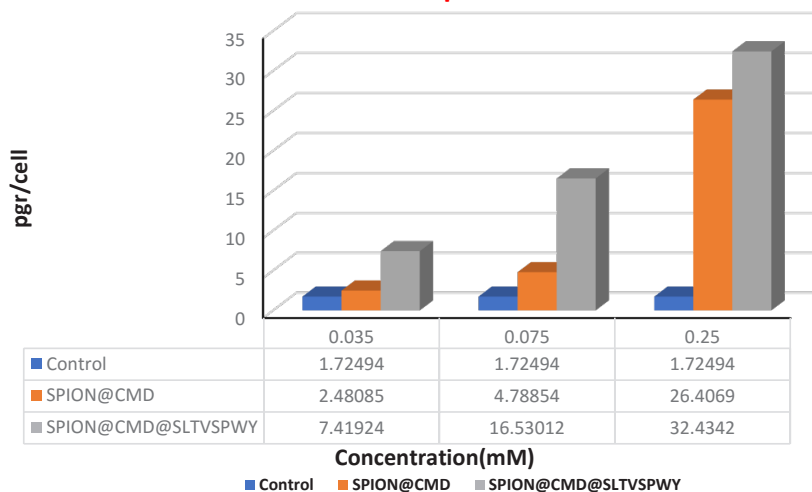


Fig 11. Cellular uptake level of synthesized nanocomplexes

in cellular uptake of targeted nanocomplexes compared to SPION@CMD. According to Fig 11, the cell uptake value for targeted nanocomplexes compared to SPION@CMD increased 3, 3.51, and 1.22-fold at concentrations 0.035, 0.075, and 0.25 mM, respectively. At concentrations greater than 0.25 mM, cells treated with SPION@CMD@SLTVSPWY showed toxicity and cell lysis after 24 hr of incubation due to the very high iron uptake of SKOV-3 cells.

**Visual evaluation of cell uptake in vitro**

As shown in Fig 12, a significant increase in iron uptake was observed in cells treated with controls (a) compared to SPION@CMD(b) and SPION@CMD@SLTVSPWY (c).

**DISCUSSION**

Cancer is one of the most important causes of death in human societies. Early detection and effective treatment of cancer are significant challenges. Molecular diagnosis of cancer in the clinic is an essential requirement. Characteristics and specific markers of tumor cells are used as targets for diagnostic and therapeutic agents (24). Her2 protein expression level is an important predictor of the diagnosis and treatment of cancer. In some cancerous tumors, especially breast cancer, there is a direct link between Her2 overexpression and mortality. (25). Based on ErbB receptor importance, many attempts have been made to improve targeted therapies (26). Heptapeptide LTVSPWY has a high binding specificity for Her2 receptors (4). Candidate structures as imaging probes must-have features such as stability and good biocompatibility. SPIONs

are low-toxic and in the long run, biodegrade to form blood hemoglobin. Their surface is covered with biocompatible materials to prevent aggregation and instability in the interstitial fluid and blood (27). Different polymers such as CD (cyclodextrin) and PEG (Polyethylene glycol) have been coated onto the surface of SPIONs to decrease their uptake by the immune system (Reticuloendothelial system) and improve their stability (28-31). According to previous studies, the surface of SPIONs can be modified with carboxyl groups (-COOH) to provide a suitable binding site for SPIONs with compounds containing amine groups (-NH<sub>2</sub>) such as peptides. (23, 32, 33). In this study, we also used the CMD (Carboxymethyl dextran) to cover the surface of nanoparticles and create carboxyl groups. Using this approach, we used carboxymethylated dextran. Forming an amide reaction with the amine group of the peptide causes the peptide to bind to the nanoparticle's

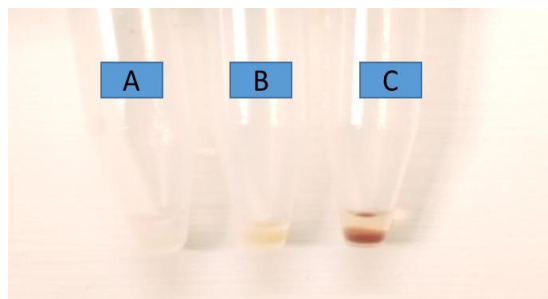


Fig 12. Observed uptake differences between nanocomplexes. control (Cell without any nanostructures) (a) SPION@CMD(b). SPION@CMD@SLTVSPWY(c).

surface. The FTIR also confirmed the formation of SPION@CMD@SLTVSPWY. The MTT test showed a lack of toxicity in the range used. There is a correlation between the size of nanostructures based on iron oxide nanoparticles with magnetic properties and cellular uptake mechanisms (34). In this study obtained average hydrodynamic diameter for nanostructures SPION@CMD and SPION@CMD@SLTVSPWY by the DLS system, which were 160.8 nm and 162.9 nm, respectively. Processing of TEM image results with Imagj software showed that the synthesized SPIONs have an average diameter of 31 nm. They also had an almost spherical and uniform morphology (35). Also, their small size and suitable surface modification led to acceptable superparamagnetic behavior (36, 37). The size reported by DLS is larger than the TEM size of the magnetic nanoparticles. This was confirmed by this research and many studies that used this method. According to previous studies, DLS for small and large particles has shown the greatest difference with TEM and the highest correspondence in medium sizes. According to other studies, the increase of DLS size also depends on the concentration of the solution containing the nanoparticles (38). The crystal size of the synthesized nanoparticles with a small size of 7.95 nm was calculated by analyzing the XRD pattern and Sherrer's equation. Comparison between DLS and TEM results shows that the average size of nanoparticles (31 nm) is composed of several crystals (3-5 crystals). However, this range of sizes is desirable to increase  $r_2$  relaxivity. (39, 40). In magnetic resonance imaging ( $T_2$ -weighted imaging) of the nanostructures concentration series (SPION@CMD and SPION@CMD@SLTVSPWY), significant negative contrast changes were observed.

The  $R_2$  value obtained with a clinical 1.5 Tesla MRI for SPION@CMD and SPION@CMD@SLTVSPWY was 318.16 and 313.26  $\text{mM}^{-1}\text{s}^{-1}$ , respectively. The results confirmed that SPION@CMD@SLTVSPWY could be considered as a targeted negative contrast agent. The relaxivity of MNPs according to equation (1) depends on the saturation magnetization ( $M_s$ ), size and shape of NPs, and the thickness of the coating:

$$R_2 = \frac{1}{T_2} = \frac{256\pi^2\gamma^2}{405} m_s^2 V \frac{r^2}{D(1 + \frac{L}{r})}$$

Where  $\chi$  is the geomagnetic ratio of protons,  $r$  is the diameter of the nanoparticles,  $m_s$  is the magnetization of a nanoparticle,  $V$  is the volume of the nanoparticles,  $D$  is the diffusion coefficient of water molecules, and  $L$  is the coating thickness of the nanoparticles (38, 41, 42). According to

equation (1),  $r_2$  decreases with the increasing diameter of the coating ( $L$ ). This confirms the relaxometry results of this study. So that, the  $r_2$  value of targeted nanocomplexes was calculated lower than  $r_2$  of SPION@CMD due to the larger diameter of the coating. The high value of the  $r_2/r_1$  ratio indicated a suitable  $T_2$  contrast agent (43). In the present study, the obtained  $r_2/r_1$  ratio showed that SPION@CMD@SLTVSPWY has the potential to be nominated as a negative contrast agent in clinical MRI. The evaluation of cellular uptake of formulations on the SKOV-3 cell line indicated the importance of SLTVSPWY peptide on the targeted formulation's uptake. In all concentrations, the cellular uptake for SPION@CMD@SLTVSPWY was higher than SPION@CMD. Moreover, the cells treated with SPION@CMD@SLTVSPWY at concentrations higher than 0.25 mM burst and lysed due to high iron uptake and intolerance. This is in agreement with previous studies in which delivery of diagnostic factors with peptides increased the cellular internalization of functionalized-SPIONs *in vitro* (17, 25, 26, 44-46). Coupling ligand (SLTVSPWY peptide) and receptor (HER2) resulted in a significant increase in endocytosis and SPION@CMD@SLTVSPWY cellular uptake in cells with HER2-overexpression (47). In the study of Zhang *et al.*, SPIONs were labeled with folate as a targeted diagnostic probe. Cell uptake experiments were performed on the SKOV-3 cell line at concentrations of 0.2 and 0.4 mM. They had the highest amount of adsorption at a concentration of 0.4 mM, approximately equal to 30  $\text{pg}/\text{cell}$ . Also, in targeted NPs with FA compared to non-targeted NPs, the amount of iron uptake in the concentrations used was approximately 2.5 and 3 times, respectively (Fig. 13) (48). However, in our study on the same cell line, the highest iron

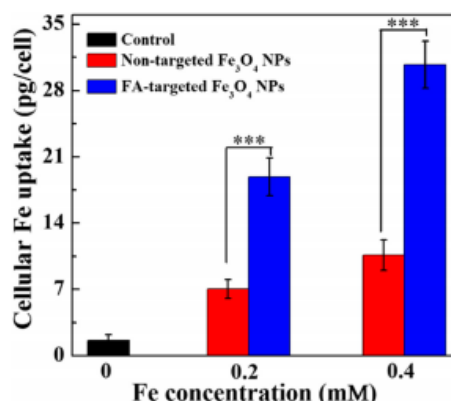


Fig 13. Cellular uptake assay of the Skov3 cells after treatment with FA-targeted SPION NPs or non-targeted SPION NPs at Fe concentration of 0.2 and 0.4 mM(48)

uptake at a concentration of 0.075 mM (5.33-fold dilution of Fe (FA-targeted SPION)) was 16.53 pg/cell. This means that SPION@CMD@SLTVSPWY is 2.93 times (approximately three times) more absorbent than FA-targeted NPs. Also, iron adsorption with targeted nanoparticles increased by 3 and 3.51 times compared to non-targeted nanoparticles at concentrations of 0.035 and 0.075 mM, respectively (Fig. 11). These results indicate that SPION@CMD@SLTVSPWY has high sensitivity and uptake in HER2-positive cells.

## CONCLUSION

This study aimed to synthesize targeted SPION-base nanoprobe to detect HER2-positive cancer cells with the help of MRI. SPIONs with an average diameter of 31 nm were synthesized using the co-precipitation method. The SPIONs were coated with CMD and labeled with SLTVSPWY peptide. The effect of nanocomplexes on Transverse relaxation time ( $T_2$ ) in aqueous solutions of varying concentrations (iron concentration) was determined with a clinical 1.5 Tesla MRI. The values  $r_2$  for SPION@CMD@SLTVSPWY and SPION@CMD were calculated as 313.26 and 318.16  $\text{mM}^{-1}\text{s}^{-1}$ , respectively, and  $r_2/r_1$  ratio for SPION@CMD@SLTVSPWY was 9.24. Targeted nanostructure (SPION@CMD@SLTVSPWY) showed higher cellular uptake than non-target (SPION@CMD). Our study suggests that SPION@CMD@SLTVSPWY can be used in the future as a targeted diagnostic probe for improving cancer HER2 positive diagnosis.

## ACKNOWLEDGEMENTS

The data presented in this report was a part of the M.Sc. thesis in the Department of Medical Physics supported by the Research Deputy of Mashhad University of Medical Sciences (Grant NO. 971200).

## CONFLICTS OF INTEREST

The authors declare no conflict of interest.

## REFERENCE

- Li ZJ, Cho CH. Peptides as targeting probes against tumor vasculature for diagnosis and drug delivery. *J Transl Med* 2012;10(1):1-9.
- Weissleder R. Molecular imaging in cancer. *Science*. 2006;312(5777):1168-1171.
- Daniels TR, Bernabeu E, Rodríguez JA, Patel S, Kozman M, Chiappetta DA, et al. The transferrin receptor and the targeted delivery of therapeutic agents against cancer. *Biochim Biophys Acta Gen Subj*. 2012;1820(3):291-317.
- Accardo A, Aloj L, Aurilio M, Morelli G, Tesaro D. Receptor binding peptides for target-selective delivery of nanoparticles encapsulated drugs. *Int J Nanomedicine*. 2014;9:1537.
- Howl J, Jones S. Insights into the molecular mechanisms of action of bioportides: a strategy to target protein-protein interactions. *Expert Rev Mol Med*. 2015;17.
- Yao L, Xu S. Detection of magnetic nanomaterials in molecular imaging and diagnosis applications. *Nanotechnol. Rev*. 2014; 3(3): 247–268.
- Weissleder R, Mahmood U. Molecular imaging. *Radiology*. 2001;219(2):316-333.
- Neve R, Lane H, Hynes N. The role of overexpressed HER2 in transformation. *Ann. Oncol*. 2001;12:S9-S13.
- Mikalauskaite A, Kondrotas R, Niaura G, Jagminas An. Gold-coated cobalt ferrite nanoparticles via methionine-induced reduction. *J. Phys. Chem. C*. 2015;119(30):17398-17407.
- Wang Z, Wang W, Bu X, Wei Z, Geng L, Wu Y, et al. Microarray based screening of peptide nano probes for HER2 positive tumor. *Anal. Chem*. 2015;87(16):8367-8372.
- Santhosh PB, Ulrich NP. Multifunctional superparamagnetic iron oxide nanoparticles: promising tools in cancer theranostics. *Cancer Lett*. 2013;336(1):8-17.
- Zhong Y, Meng F, Deng C, Zhong Z. Ligand-directed active tumor-targeting polymeric nanoparticles for cancer chemotherapy. *Biomacromolecules*. 2014;15(6):1955-1969.
- Dai T, Li N, Zhang L, Zhang Y, Liu Q. a new target ligand ser-glu for PePT1-overexpressing cancer imaging. *Int. J. Nanomed*. 2016;11:203.
- Shadidi M, Sioud M. Identification of novel carrier peptides for the specific delivery of therapeutics into cancer cells. *FASEB J*. 2003;17(2):256-258.
- Khodadust F, Ahmadpour S, Aligholikhamesh N, Abedi S, Hosseini-mehr S. Corrigendum to " An Improved 99m Tc-HYNIC-(Ser) 3-LTVSPWY Peptide With EDDA/tricine as Co-Ligands for Targeting and Imaging of HER2 Overexpression Tumor. *Eur. J. Med. Chem*. 2018;157:782.
- Meschenmoser K, Kim Y, Franken S, Nowak M, Feldmann G, Bendas G, et al. Targeting cancer with a bi-functional peptide: *in vitro* and *in vivo* results. *in vivo*. 2013;27(4):431-442.
- Rahmanian N, Hosseini-mehr SJ, Khalaj A, Noaparast Z, Abedi SM, Sabzevari O. 99m Tc labeled HYNIC-EDDA/tricine-GE11 peptide as a successful tumor targeting agent. *Med Chem Res*. 2018;27(3):890-902.
- Aligholikhamesh N, Ahmadpour S, Khodadust F, Abedi SM, Hosseini-mehr SJ. 99mTc-HYNIC-(Ser) 3-LTVSPWY peptide bearing tricine as co-ligand for targeting and imaging of HER2 overexpression tumor. *Radiochim Acta*. 2018;106(7):601-609.
- Wang XF, Birringer M, Dong LF, Low P, Swettenham E, Stantic M, et al. A Peptide Conjugate of Vitamin E Succinate Targets Breast Cancer Cells with High ErbB2 Expression. *Cancer Res*. 2007;67(7):3337-3344.
- Shahsavari S, Shaghghi Z, Abedi SM, Hosseini-mehr SJ. Evaluation of 99mTc-HYNIC-(ser) 3-LTVSPWY peptide for glioblastoma imaging. *Int. J. Radiat. Biol*. 2020; 96(4):502-509.
- Yan G-P, Robinson L, Hogg P. Magnetic resonance imaging contrast agents: overview and perspectives. *Radiography*. 2007;13:e5-e19.
- Lawaczeck R, Menzel M, Pietsch H. Superparamagnetic iron oxide particles: contrast media for magnetic resonance imaging. *Appl. Organomet. Chem*. 2004;18(10):506-513.
- Yousefvand M, Mohammadi Z, Ghorbani F, Irajirad R, Abedi H, Seyedi S, et al. Investigation of Specific Targeting

- of Triptorelin-Conjugated Dextran-Coated Magnetite Nanoparticles as a Targeted Probe in GnRH+ Cancer Cells in MRI. *Contrast Media Mol. Imaging*. 2021;1-10
24. Liu R, Li X, Xiao W, Lam KS. Tumor-targeting peptides from combinatorial libraries. *Adv. Drug Deliv. Rev.* 2017;110:13-37.
  25. Khodadust F, Ahmadpour S, Aligholikhamesh N, Abedi SM, Hosseinimehr SJ. An improved 99mTc-HYNIC-(Ser) 3-LTVSPWY peptide with EDDA/tricine as co-ligands for targeting and imaging of HER2 overexpression tumor. *Eur. J. Med. Chem.* 2018;144:767-773.
  26. Hagimori M, Fuchigami Y, Kawakami S. Peptide-based cancer-targeted DDS and molecular imaging. *Chem. Pharm. Bull.* 2017;65(7):618-624.
  27. Sakulkhu U, Mahmoudi M, Maurizi L, Coullerez G, Hofmann-Antenbrink M, Vries M, et al. Significance of surface charge and shell material of superparamagnetic iron oxide nanoparticle (SPION) based core/shell nanoparticles on the composition of the protein corona. *Biomater. Sci.* 2015;3(2):265-278.
  28. Hayashi K, Nakamura M, Sakamoto W, Yogo T, Miki H, Ozaki S, et al. Superparamagnetic nanoparticle clusters for cancer theranostics combining magnetic resonance imaging and hyperthermia treatment. *Theranostics*. 2013;3(6):366.
  29. Li J, Hu Y, Yang J, Sun W, Cai H, Wei P, et al. Facile synthesis of folic acid-functionalized iron oxide nanoparticles with ultrahigh relaxivity for targeted tumor MR imaging. *J. Mater. Chem. B.* 2015;3(28):5720-5730.
  30. Hao R, Yu J, Ge Z, Zhao L, Sheng F, Xu L, et al. Developing Fe<sub>3</sub>O<sub>4</sub> nanoparticles into an efficient multimodality imaging and therapeutic probe. *Nanoscale*. 2013;5(23):11954-11963.
  31. Yen SK, Padmanabhan P, Selvan ST. Multifunctional iron oxide nanoparticles for diagnostics, therapy and macromolecule delivery. *Theranostics*. 2013;3(12):986.
  32. Hong SC, Lee JH, Lee J, Kim HY, Park JY, Cho J, et al. Subtle cytotoxicity and genotoxicity differences in superparamagnetic iron oxide nanoparticles coated with various functional groups. *Int J Nanomedicine*. 2011;6:3219-3231.
  33. Singh H, Du J, Singh P, Mavlonov GT, Yi TH. Development of superparamagnetic iron oxide nanoparticles via direct conjugation with ginsenosides and its in-vitro study. *J. Photochem. Photobiol. B: Biol.* 2018;185:100-110.
  34. Thomas R, Park I-K, Jeong YY. Magnetic iron oxide nanoparticles for multimodal imaging and therapy of cancer. *Int J Mol Sci.* 2013;14(8):15910-15930.
  35. Joseph AM, Thangaraj B, Gomathi RS, Adaikalam AAR. Synthesis and characterization of cobalt ferrite magnetic nanoparticles coated with polyethylene glycol. *AdvNanoBioM&D*. 2017;1(1):71-77.
  36. Ishizaki T, Yatsugi K, Akedo K. Effect of particle size on the magnetic properties of Ni nanoparticles synthesized with trioctylphosphine as the capping agent. *Nanomaterials*. 2016;6(9):172.
  37. Sheng Y, Liao LD, Thakor NV, Tan MC. Nanoparticles for molecular imaging. *J Biomed Nanotechnol.* 2014;10(10):2641-2676.
  38. Kostevšek N. A review on the optimal design of magnetic nanoparticle-based T2 MRI contrast agents. *Magnetochemistry*. 2020;6(1):11.
  39. Abd Elrahman AA, Mansour FR. Targeted magnetic iron oxide nanoparticles: Preparation, functionalization and biomedical application. *J Drug Deliv Sci Technol.* 2019;52:702-712.
  40. Huang C-C, Chuang K-Y, Chou C-P, Wu M-T, Sheu H-S, Shieh D-B, et al. Size-control synthesis of structure deficient truncated octahedral Fe<sub>3</sub>-δO<sub>4</sub> nanoparticles: high magnetization magnetites as effective hepatic contrast agents. *J. Mater. Chem.* 2011;21(20):7472-7479.
  41. Jun Y-w, Huh Y-M, Choi J-s, Lee J-H, Song H-T, Kim S, et al. Nanoscale size effect of magnetic nanocrystals and their utilization for cancer diagnosis via magnetic resonance imaging. *J. Am. Chem. Soc.* 2005;127(16):5732-5733.
  42. Kang J, Lee H, Kim Y-N, Yeom A, Jeong H, Lim YT, et al. Size-regulated group separation of CoFe<sub>2</sub>O<sub>4</sub> nanoparticles using centrifuge and their magnetic resonance contrast properties. *Nanoscale Res. Lett.* 2013;8(1):1-7.
  43. Issa B, Obaidat IM, Albiss BA, Haik Y. Magnetic nanoparticles: surface effects and properties related to biomedicine applications. *International journal of molecular sciences*. 2013;14(11):21266-21305.
  44. Nitin N, LaConte L, Zurkiya O, Hu X, Bao G. Functionalization and peptide-based delivery of magnetic nanoparticles as an intracellular MRI contrast agent. *J Biol Inorg Chem.* 2004;9(6):706-712.
  45. Ahmadpour S, Noaparast Z, Abedi SM, Hosseinimehr SJ. 99m Tc-HYNIC-(tricine/EDDA)-FROP peptide for MCF-7 breast tumor targeting and imaging. *J Biomed Sci.* 2018;25(1):1-11.
  46. Jie L-Y, Cai L-L, Wang L-J, Ying X-Y, Yu R-S, Zhang M-M, et al. Actively-targeted LTVSPWY peptide-modified magnetic nanoparticles for tumor imaging. *Int J Nanomedicine*. 2012;7:3981-3989.
  47. Liu R, Li X, Xiao W, Lam KS. Tumor-targeting peptides from combinatorial libraries. *Adv Drug Deliv Rev.* 2017;110(111):13-37.
  48. Zhang H, Li J, Hu Y, Shen M, Shi X, Zhang G. Folic acid-targeted iron oxide nanoparticles as contrast agents for magnetic resonance imaging of human ovarian cancer. *J Ovarian Res.* 2016;9(1):1-8.